Ventricular Septal Defect

3

Contents

3.1 Anatomy and Haemodynamics

The ventricular septum is a complex structure composed of several different portions. These components include the inlet septum adjacent to the atrioventricular valves, the trabecular septum extending to the apex of the ventricles, the membranous part of the ventricular septum and the outlet septum separating aortic and pulmonary outlet. Ventricular septal defects are described according to their size and their location and extension within the different parts of the ventricular septum. While the location of the VSD is important with regard to surgical procedures, the size of the defect defines its haemodynamic relevance.

Ventricular septal defects are the most frequent cardiac malformation accounting for 48.9 % of congenital heart defects reported in the German PAN study (Lindinger et al. 2010; Schwedler et al. 2011). A considerable percentage, representing about two-thirds of these defects, is muscular and small (Lindinger et al. 2010).

There has been extensive debate in the literature concerning the nomenclature of ventricular septal defects, according to their different locations. The different nomenclature systems have been summarized by the congenital heart surgery nomenclature and database project (Jacobs et al. 2000). According to the location of the defect, four types are differentiated plus the rare Gerbode-type defects, which allow a direct communication between the left ventricle and left atrium (Jacobs et al. 2000). The four types of defects are:subarterial, perimembranous, inlet and muscular (Fig. 3.1).

- Type 1 *subarterial defects* (synonymous with supracristal, conal or infundibular ventricular septal defects) are located beneath the semilunar valves in the conal or outlet septum. They can be further differentiated into subarterial defects within the conal or infundibular septum completely surrounded by muscle, so-called *conal muscular* defects (Jacobs et al. 2000). Defects, which miss a superior muscular border and therefore are not separated from

Electronic supplementary material The online version of this chapter (doi:10.1007/978-3-319-42919-9_3) contains supplementary material, which is available to authorized users.

M. Hofbeck et al., *Doppler Echocardiography in Infancy and Childhood*, DOI 10.1007/978-3-319-42919-9_3

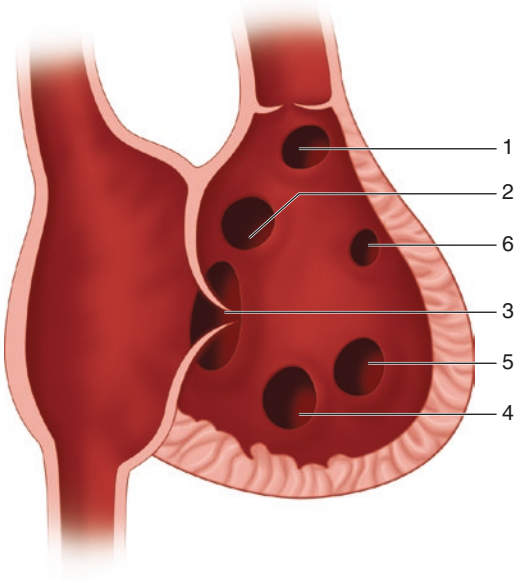

Fig. 3.1 The schematic anterior view of the right ventricle shows different locations of ventricular septal defects including subarterial defects (*1*), perimembranous defects (*2*) and inlet defects (*3*). Muscular VSDs can be located in the posterior and inferior muscular septum (*4*), in the trabecular portion (*5*) or in the outlet septum (*6*)

the semilunar valves, are termed *juxtaarterial* or *doubly committed*.

- Type 2 defects involving the membranous septum and bordered by an atrioventricular valve are termed *perimembranous VSD* (synonyms paramembranous, conoventricular VSD). This type of VSD may extend towards the inlet, trabecular or outlet portion of the septum. Perimembranous defects that extend towards the outlet portion of the septum may be associated with *malalignment of the conal septum*. This malalignment can be *anterior* resulting in a tetralogy of Fallot-type malalignment of the conal septum, or it can be *posterior* resulting in an interrupted aortic arch type of malalignment (see also Chaps. 11 and 22).
- Type 3 defects are termed *inlet VSD* or AV canal type VSD and involve the inlet of the right ventricular septum immediately inferior to the AV valve apparatus (Jacobs et al. 2000). It may be associated with an AVSD (AV canal defect) or occur as a separate lesion.
- Type 4 *muscular VSD* refers to those defects that are surrounded entirely by musculature. These can be subspecified according to their location in different parts of the muscular septum. *Muscular inlet* (synonym posterior) defects are located in the inlet portion of the ventricular septum, separated from the atrioventricular valves by muscular tissue. Other locations are *muscular trabecular* defects in the trabecular portion and *muscular outlet* in the outlet portion of the septum. The trabecular defects are further subspecified into anterior, apical and midventricular defects. Muscular defects may be large and confluent or multiple. The term multiple or Swiss cheese is suggested for patients with more than three muscular VSDs (Jacobs et al. 2000).

Large ventricular septal defects allow transmission of the systemic left ventricular pressure to the right ventricle and the pulmonary vascular bed. Therefore pulmonary hypertension is present in patients with large defects starting from birth. Shunting across the VSD and the development of clinical symptoms depend on the relation of pulmonary and systemic vascular resistance. Since pulmonary vascular resistance is physiologically high in the neonatal period, there is only a small amount of LR-shunting, even in the presence of a large defect. Because of that, isolated ventricular septal defects almost never are responsible for clinical symptoms in the first weeks of life. This has to be taken into account in the clinical and in the echocardiographic evaluation of neonates with VSD: there may be only a faint systolic murmur and absence of congestive heart failure. Due to the absence of significant shunting, it may be difficult to detect the defect by colour Doppler interrogation of the ventricular septum. Therefore echocardiography has to focus on careful screening of the ventricular septum by two-dimensional echocardiography.

Physiological decrease in pulmonary vascular resistance during the first weeks of life results in a continuing increase of left to right shunt with consecutive volume load of the left heart, frequently accompanied by clinical signs of congestive heart failure. With increasing age, the pulmonary vascular bed reacts with vasoconstriction resulting in an increase of pulmonary vascular resistance. This increase in pulmonary vascular resistance results in a decrease of left to right shunting accompanied frequently by an improvement of the clinical signs of congestive heart failure.

Moderate-size ventricular septal defects do not allow equalization of right and left ventricular pressures. Therefore these patients are not confronted with pulmonary hypertension and the risk of development of pulmonary vascular changes during the first years of life. Nevertheless moderate-size VSDs are large enough to allow significant left to right shunting with possible development of congestive heart failure and failure to thrive.

Small defects as well do not allow transmission of systolic pressure to the right ventricle: due to the small size of the defect, they allow only a minor amount of left to right shunting that has neither negative effects on the pulmonary vascular bed nor produces clinical symptoms except for the presence of a systolic murmur. In the presence of the elevated pulmonary vascular resistance in the neonatal period, there may be almost no shunting across small defects resulting in absence of a clinically detectable murmur. Due to the absence of shunting, it may be difficult to detect these defects by CDE during the first days of life. Spontaneous reduction of pulmonary vascular resistance in the second and third week of life results in the appearance of a high-pitched systolic murmur and left to right shunting across the defect that

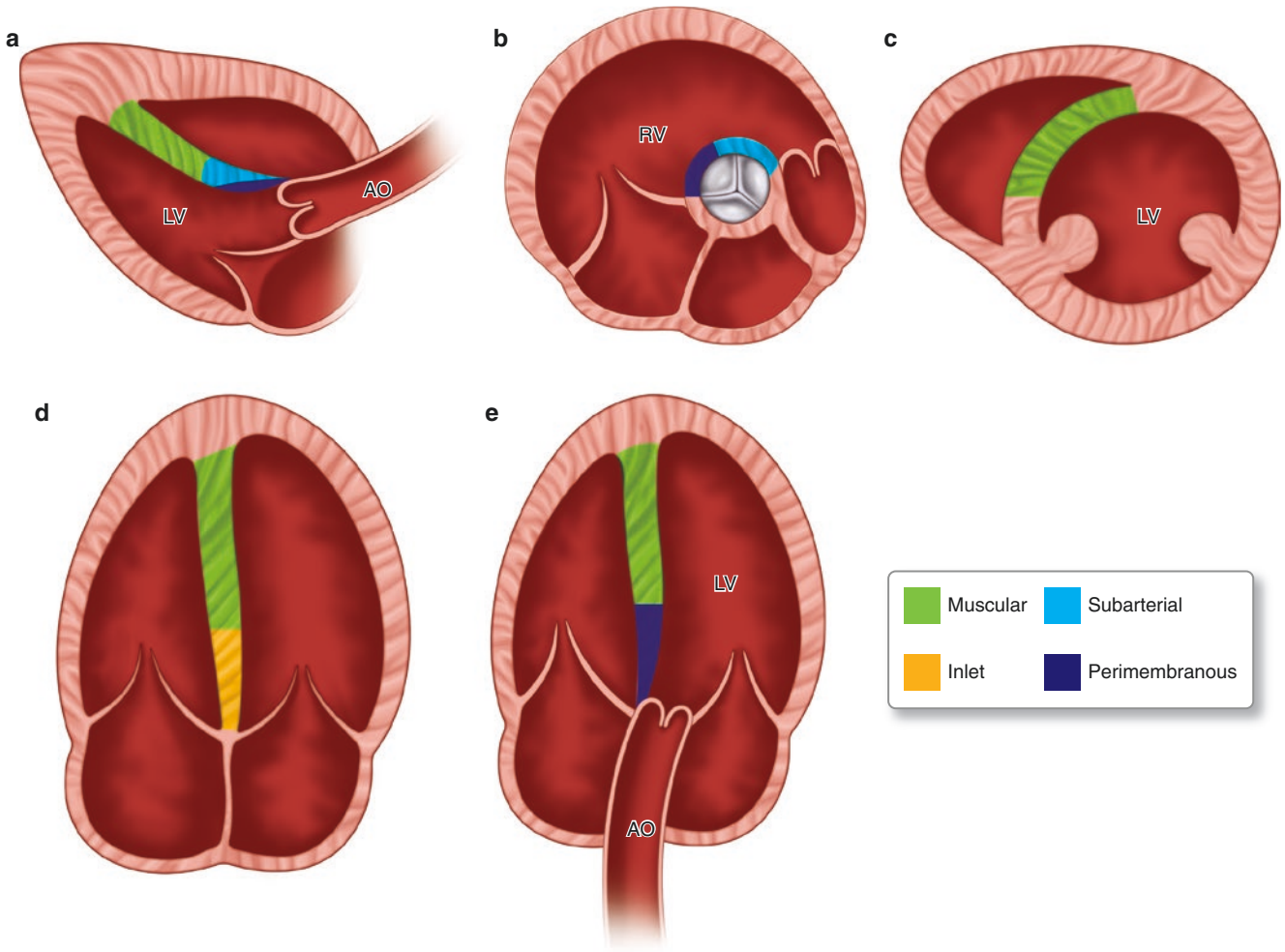

Fig. 3.2 This diagram shows the location of different types of VSD in the parasternal long-axis view (**a**), in the parasternal short-axis view of the base of the heart (**b**) and of the midventricular septum (**c**) and in the apical four-chamber (**d**) and five-chamber view (**e**). Since none of the echocardiographic planes depicts the entire ventricular septum, echocardiographic examination of the ventricular septum always requires the application of multiple planes (The diagram has been modified according to Deeg K.H., Singer, H. Echokardiographische Diagnose des Ventrikelseptumdefektes, derkinderarzt 22,799 (1991). With kind permission from Hansisches Verlagskontor GmbH)

can be detected easily by colour Doppler interrogation of the ventricular septum due to the high velocity of the jet.

Ventricular septal defects are frequently associated with additional cardiovascular malformations, e.g. pulmonary valvular stenosis or coarctation of the aorta. Furthermore they may be an integral part of complex congenital cardiac malformations like tetralogy of Fallot, pulmonary atresia and VSD, truncus arteriosus or double outlet right ventricle.

3.2 Two-Dimensional Echocardiography

Two-dimensional echocardiography has to define the location, extension and size of the defect. Furthermore it is important to address the relation of the defect to adjacent structures, especially the atrioventricular and the semilunar valves (Baker et al. 1988; Capelli et al. 1983; Nygren et al. 2000; Sutherland et al. 1982).

It should always be kept in mind that more than one VSD may be present in the same or in different parts of the ventricular septum. Since the ventricular septum does not represent a linear structure, echocardiographic description of ventricular septal defects requires the application of a variety of different precordial and subcostal views. The optimal planes for visualization of defects differ significantly between defects in different parts of the ventricular septum (Fig. 3.2).

Perimembranous VSDs are located just underneath the septal leaflet of the tricuspid valve, and from the left ventricular aspect, they lie underneath the aortic valve. Description of these defects should include information concerning their size as well as possible extension of the defect into other portions of the ventricular septum including the inlet, trabecular and outlet portions. The most informative plane for the detection of these defects is the parasternal short axis of the left ventricular outflow tract.

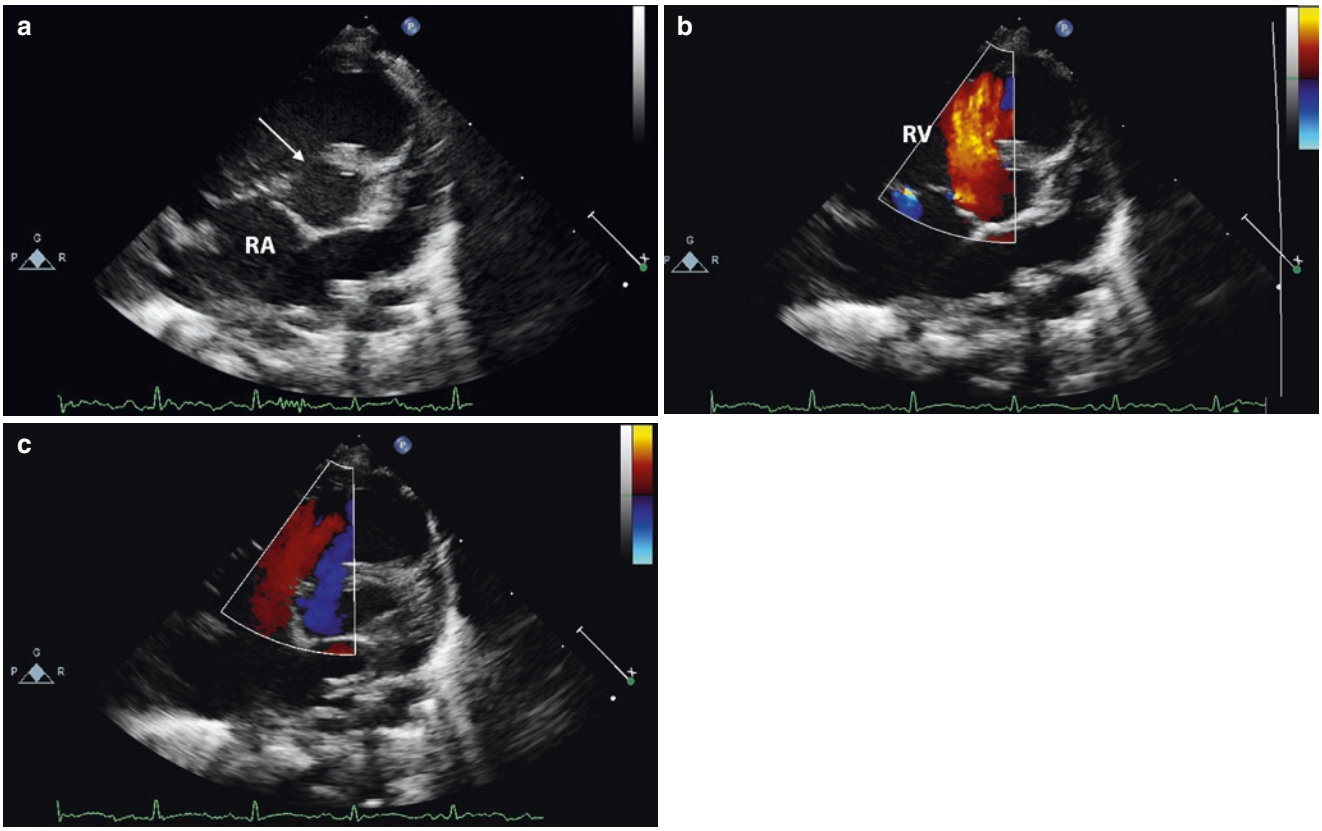

Fig. 3.3 Large perimembranous VSD (*arrow*) in the parasternal short-axis view (**a**). Colour Doppler displays LR-shunting during systole (**b**) and some RL-shunting in diastole (**c**). *RA* right atrium, *RV* right ventricle

In this plane, perimembranous VSDs are located at 9–11 o'clock (Fig. 3.3, Videos 3.1 and 3.2). In the apical four-chamber view, perimembranous VSDs can be visualized following anterior tilt of the transducer into the apical five-chamber view (Fig. 3.4, Videos 3.3 and 3.4). In this plane, slight clockwise rotation of the transducer opens the left ventricular outflow tract and shows the distance of the VSD to the aortic valve. This view will also show possible subaortic stenosis by a fibromuscular membrane, if present. Perimembranous ventricular septal defects may undergo spontaneous decrease in size or even spontaneous closure (Penny and Vick 2011). This process is frequently due to accessory tricuspid valve tissue covering the defect. Echocardiography can display the decrease in size as well as the underlying mechanism (Fig. 3.4, Videos 3.5 and 3.6). In the parasternal long-axis view, perimembranous VSDs are localized underneath the aortic valve (Videos 3.7 and 3.8). In this plane, however, large defects may remain undetected, if they are located laterally to the scanning plane (Fig. 3.5). From the subcostal window, perimembranous VSDs can be visualized in the coronal view of the left ventricular outflow tract. In analogy to left ventricular angiography, VSDs in this view are visualized underneath the aortic valve (Fig. 3.6). True Gerbode defects, connecting the left ventricle directly to the right atrium, are exceedingly rare. However in patients with perimembranous VSD, it is not too uncommon to detect shunting from the left ventricle to the right atrium (Kelle et al. 2009; Leung et al. 1986): accessory tricuspid valve tissue, which partially obstructs the perimembranous VSD, may direct part of the jet from the left ventricle to the right atrium (Fig. 3.7). Since this jet entering the right atrium originates from the left ventricle, its maximal velocity reflects the pressure difference between the left ventricle and right atrium. If it is used for calculation of right ventricular pressure based on the modified Bernoulli equation, this will result in significant overestimation.

Perimembranous ventricular septal defects extending towards the outlet septum, associated with malalignment of the conal (outlet) septum, are termed malalignment VSD. Malalignment ventricular septal defects can be associated either with anterior or posterior deviation of the outlet septum. Defects with anterior deviation of the outlet septum, which are typically found in patients with tetralogy of Fallot, are well depicted in the parasternal short axis (Fig. 3.8, Video 3.9). Depending on the degree of anterior deviation, the outlet septum may cause significant subpulmonary obstruction. The parasternal short-axis view displays both the VSD and the obstruction of the right ventricular outflow tract by the deviated outlet septum. In the parasternal long-axis view, these defects are located

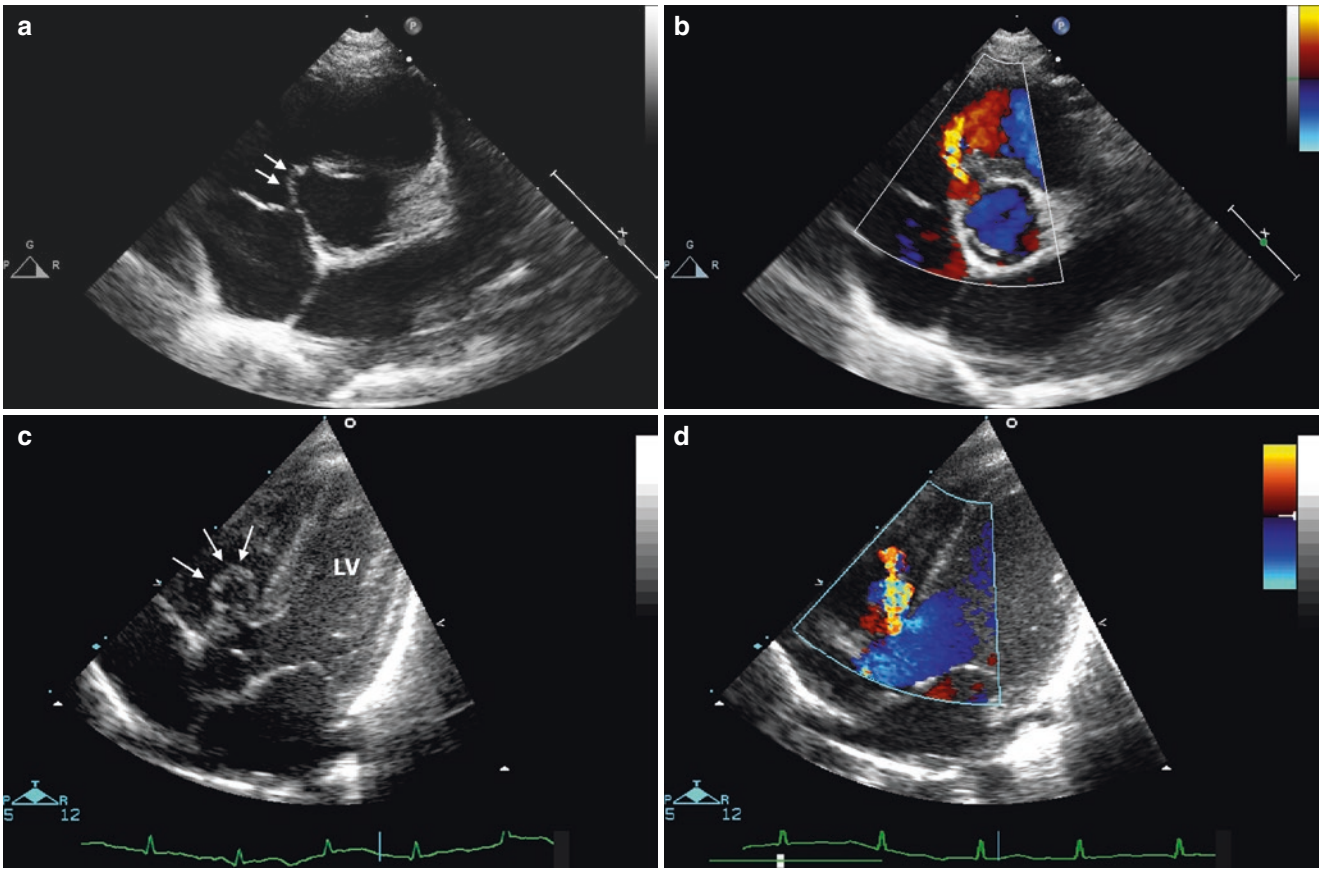

Fig. 3.4 Parasternal short-axis view showing restriction of a perimembranous VSD (*arrows*) due to accessory tricuspid valve tissue (**a**). Colour Doppler confirms a small amount of LR-shunting (**b**). Aneurysmal tricuspid valve tissue (*arrows*) obstructing a perimembranous VSD in the apical five-chamber view (**c**) with little LR-shunting on colour Doppler (**d**). LV left ventricle

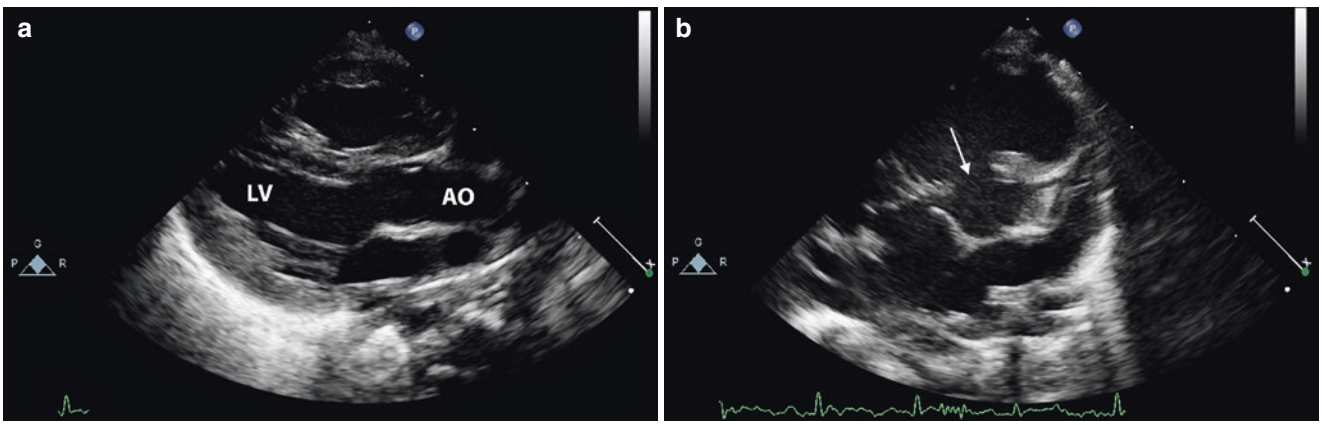

Fig. 3.5 Parasternal long-axis view failing to visualize a large VSD, since the plane of examination is too far to the left (**a**). The defect is obvious (*arrow*) in the parasternal short-axis view (**b**). *LV* left ventricle, *AO* aorta

immediately underneath the aortic valve (Fig. 3.9, Videos 3.10 and 3.11). Frequently there is at least some degree of dextroposition of the aorta, resulting in overriding over the VSD. In the apical four-chamber view, the ventricular septum may appear intact in the posterior and intermediate planes (Fig. 3.9). Visualization of anterior malalignment VSDs requires tilting of the transducer to an anterior plane (Video 3.12). Another plane that allows clear visualization of these VSDs together with the anterior deviation of the outlet septum is the subcostal RAO view (Fig. 3.10, Video 3.13), while anterior deviation of the outlet septum is well depicted in the subcostal sagittal view (Video 3.14).

Posterior deviation of the outlet septum resulting in obstruction of the left ventricular outflow tract can be well

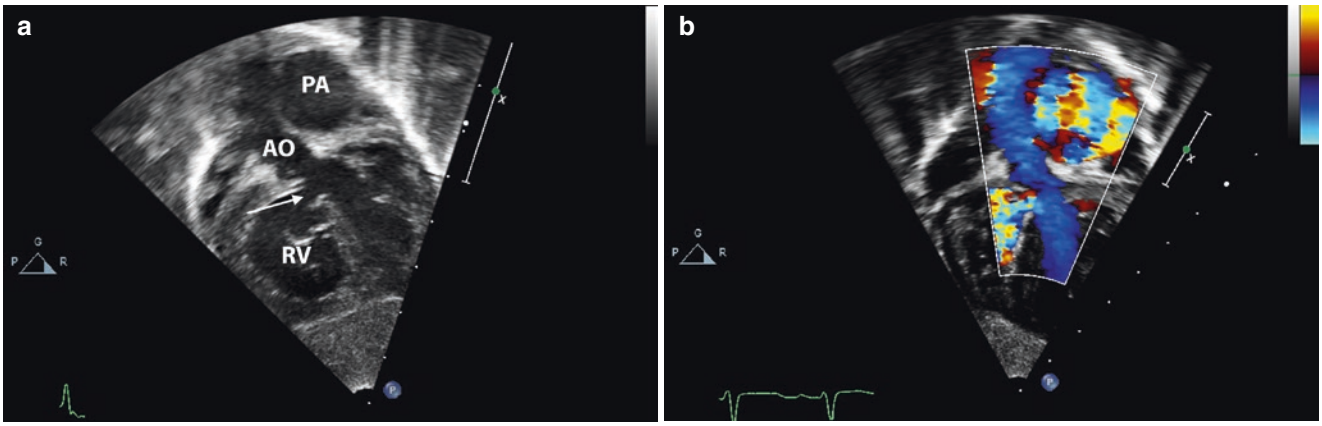

Fig. 3.6 Large perimembranous VSD (*arrow*) visualized in the subcostal coronal view (**a**) depicting its proximity to the aortic valve (AO). Colour Doppler displays LR-shunting across the VSD (**b**). *PA* pulmonary artery, *RV* right ventricle

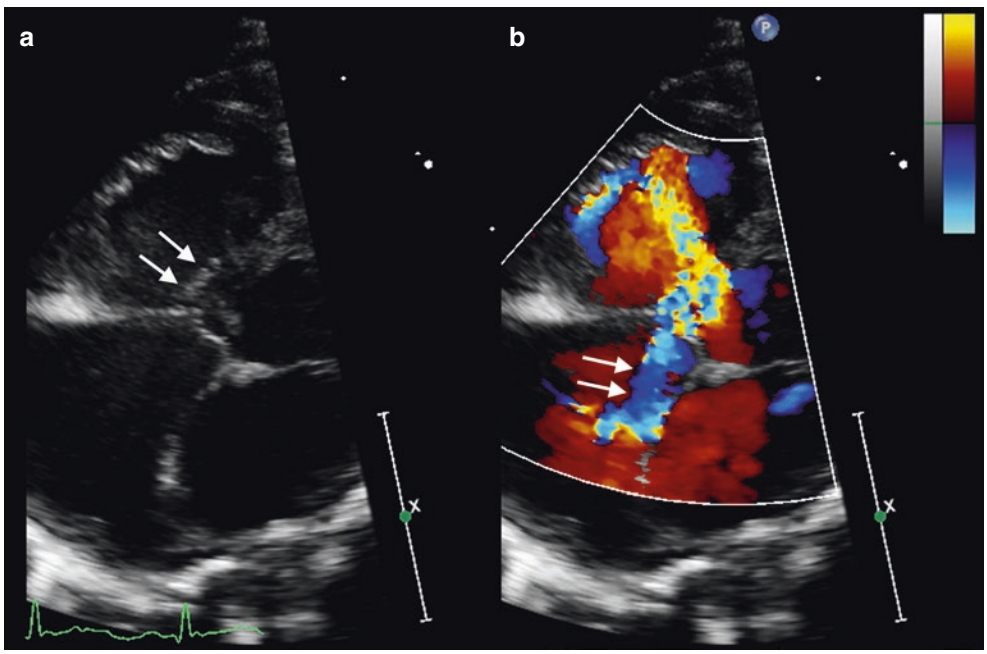

Fig. 3.7 Perimembranous VSD with reduction of its size (*arrows*) by accessory tricuspid valve tissue (**a**). The jet across the VSD is partially deflected by the tricuspid valve tissue (*arrow*) to the right atrium resulting in left ventricular to right atrial shunting (**b**)

displayed in the parasternal long axis (Fig. 3.11, Videos 3.15 and 3.16). Malalignment ventricular septal defects with posterior deviation of the infundibular septum are typically found in patients with aortic arch obstruction, especially IAA type B (Kaulitz et al. 1999; Smallhorn et al. 1982). Posterior deviation of the outlet septum is also evident in the apical five-chamber view (Fig. 3.11).

Visualization of muscular ventricular septal defects by 2D echo is somewhat limited, since the right ventricular opening of muscular defects is rather difficult to localize among the trabeculations of the muscular trabecular septum. Echocardiographic diagnosis especially of small muscular defects is a domain of colour Doppler echocardiography (Ludomirsky et al. 1986). Therefore echocardiographic diagnosis of muscular defects will be addressed in the chapter colour Doppler.

The best plane for visualization of inlet defects is the apical four-chamber view (Fig. 3.12). They may occur as isolated defects or in the more complex context of atrioventricular septal defects (Jacobs et al. 2000). Since the latter belong to a separate entity, they will be addressed in Chap. 4. Inlet ventricular septal defects are located posteriorly as compared to perimembranous VSDs and may be associated with straddling of either of the atrioventricular valves (Fig. 3.12, Video 3.17).

Subarterial (synonym supracristal, conal or infundibular) ventricular septal defects, which are located in the outlet (conal) septum, can be depicted in the parasternal short-axis view of the left ventricular outflow tract

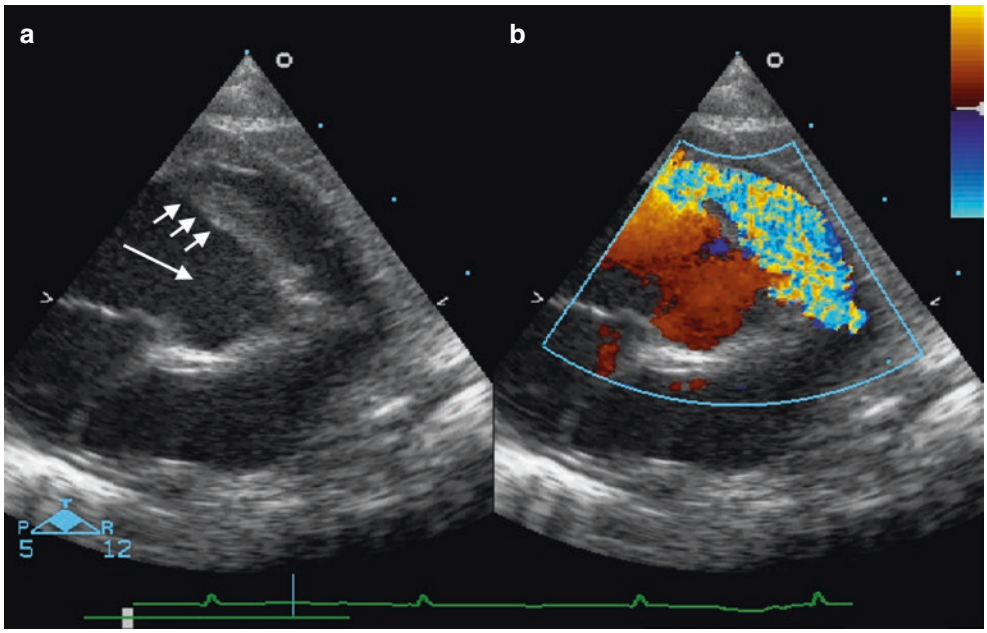

Fig. 3.8 Large malalignment VSD with anterior deviation of the outlet septum in the parasternal short axis (**a**). Colour Doppler shows acceleration of blood flow due to significant narrowing of the pulmonary outflow tract (**b**)

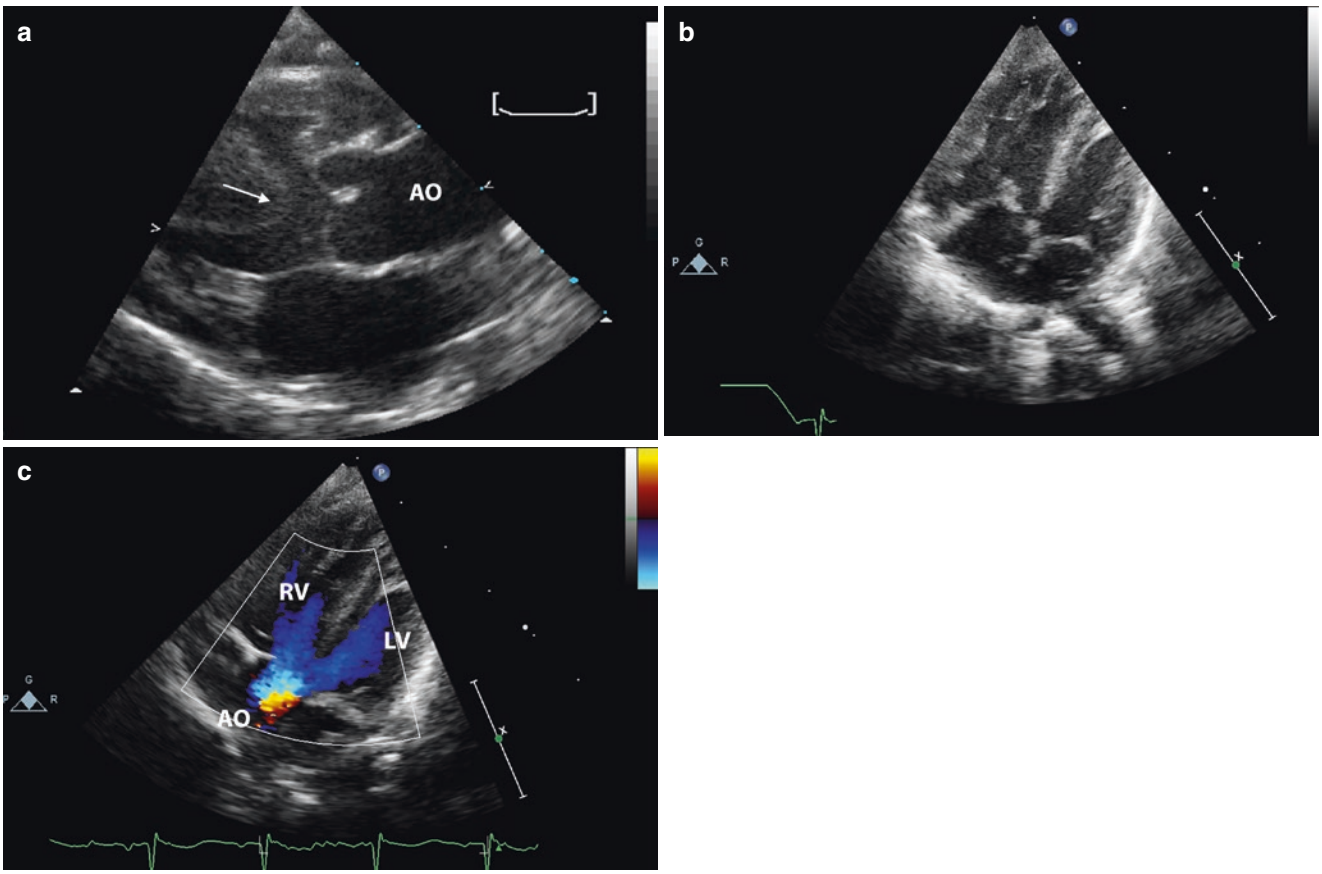

Fig. 3.9 The parasternal long axis (**a**) in this patient with malalignment VSD and tetralogy of Fallot shows overriding of the aorta over the ventricular septum (*arrow*); despite its size the malalignment VSD is not apparent in the apical four-chamber view (**b**); following ventral tilt of the transducer, colour Doppler in the five-chamber view clearly shows shunting from both ventricles into the overriding aorta (**c**). *AO* aorta, *LV* left ventricle, *RV* right ventricle

(Fig. 3.13, Videos 3.18 and 3.19). According to their location in the outlet septum, they may be separated from the semilunar valves by a muscular rim (conal muscular subarterial VSD), or they may be adjacent directly to the semilunar valves representing a juxtaarterial or doubly committed VSD (Jacobs et al. 2000). In the latter defects, there is a direct continuity between the aortic and pulmonary valve (Fig. 3.13, Videos 3.18 and 3.19). While doubly committed VSD in the parasternal short-axis view is located at 12–2 o'clock, in the parasternal long-axis view, these defects extend up to the aortic valve with the right cusp of the aortic valve representing the upper border of the defect (Figs. 3.13 and 3.14, Videos 3.20 and 3.21). Due to the close proximity of this cusp to the defect, patients with subarterial VSD carry a significant risk for development of aortic valve prolapse with consecutive aortic valve regurgitation (Butter et al. 1998; Craig et al. 1986; Momma et al. 1984; Rhodes et al. 1990; Yoshimura et al. 2010). Careful inspection of the aortic valve in the parasternal long and short axis is therefore required in these patients to detect early signs of incipient prolapse (Craig et al. 1986; Momma et al. 1984; Schmidt et al. 1988; Tweddell et al. 2006).

Irrespective of the localization of the ventricular septal defect, assessment of the size of the ventricles and atria gives some information about the haemodynamic impact of the defect. Small defects without haemodynamic significance present with normal-size atria and ventricles. Defects, associated with significant LR-shunt, result in an enlargement of the pulmonary artery, left atrium and left ventricle, since the recirculating blood results in a significant volume load for the pulmonary circulation and left heart (Fig. 3.15, Video 3.22). This applies for medium-size or large defects, as long as there is no significant elevation of pulmonary vascular resistance. With increasing pulmonary vascular resistance, the signs of left ventricular volume load diminish, and right ventricular hypertrophy and enlargement develop, due to the increasing pressure load of the right ventricle (Fig. 3.15).

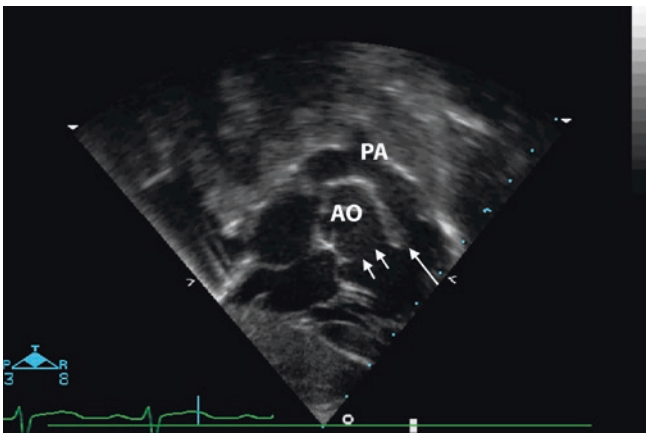

Fig. 3.10 The subcostal RAO view in this patient with malalignment defect shows nicely the large defect (*small arrows*) and the deviation of the outlet septum (*large arrow*). *AO* aorta, *PA* pulmonary artery

3.3 Colour Doppler Echocardiography

Colour Doppler examination plays a vital role in the detection and assessment of VSDs. On one hand, it allows definite confirmation of the presence and localization of suspected defects. This applies specifically for defects in the muscular portion of the ventricular septum, where small- and medium-size defect may hide behind the heavily trabeculated right ventricular surface of the septum (Ludomirsky et al. 1986).

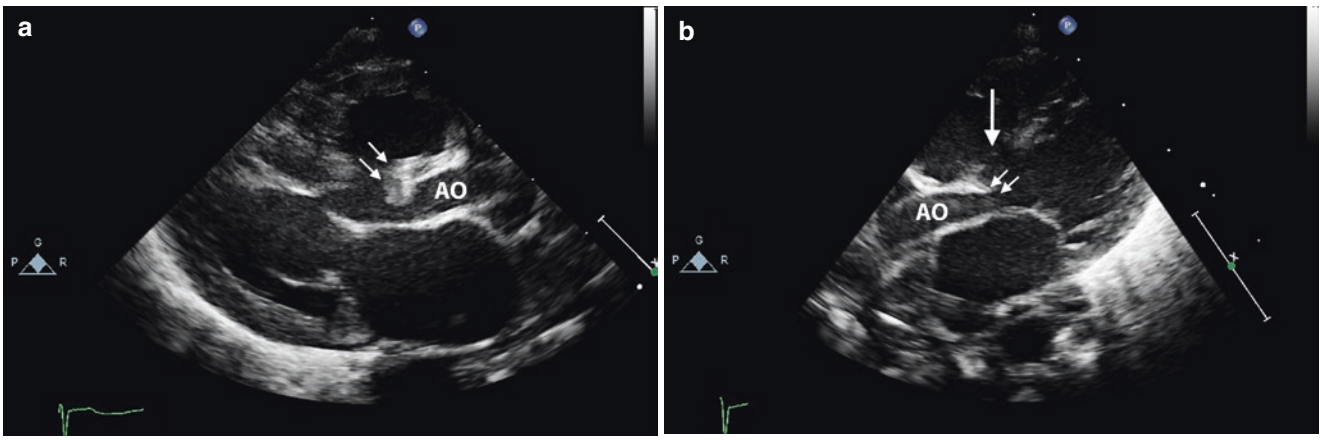

Fig. 3.11 The parasternal long axis (**a**) in this patient with malalignment VSD shows posterior deviation of the outlet septum (*arrows*) obstructing the left ventricular outflow tract underneath the aortic valve (*AO*). The apical five-chamber view in the same patient (**b**) shows the large VSD (*large arrow*) and obstruction of the left ventricular outflow by the outlet septum (*small arrows*)

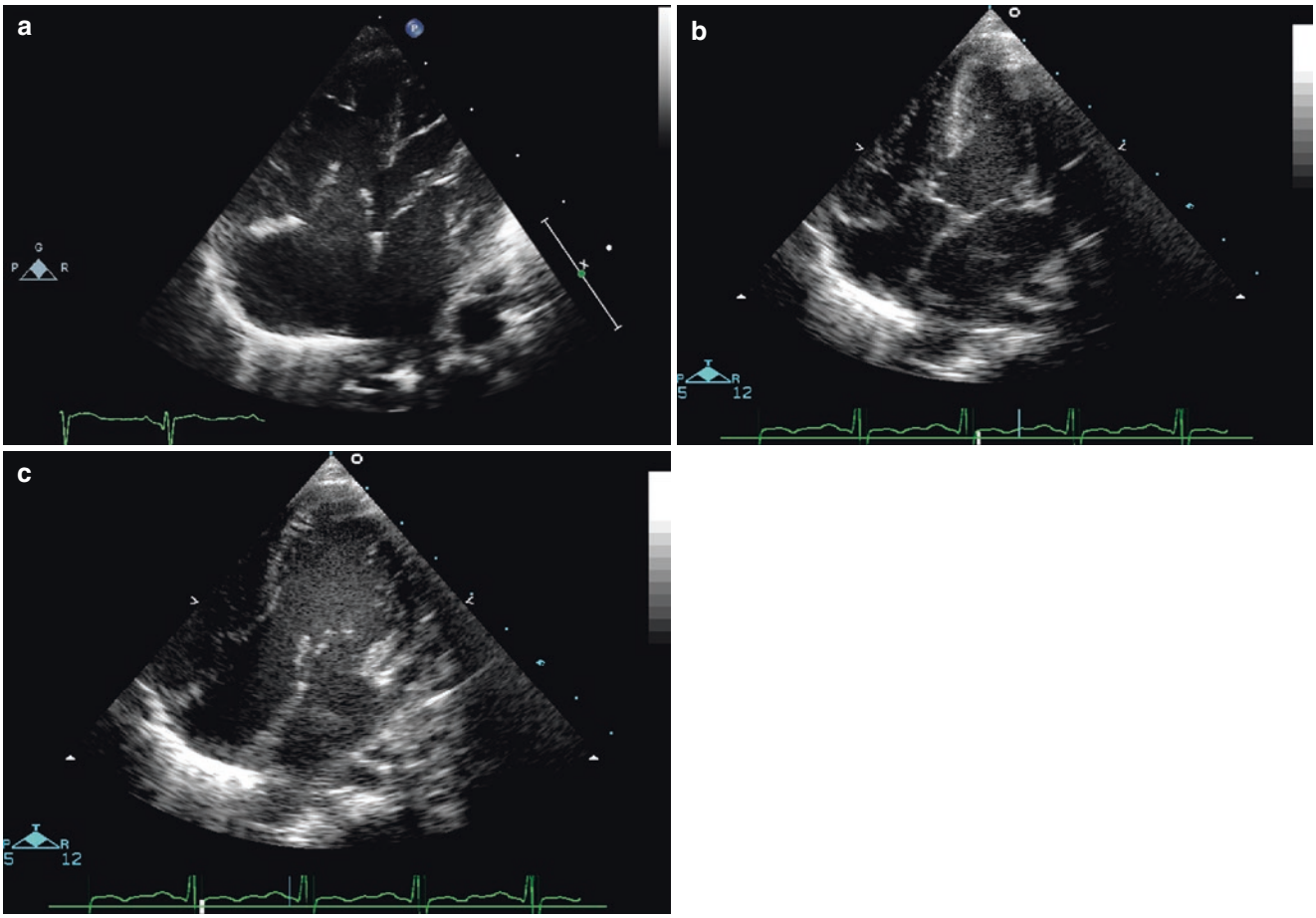

Fig. 3.12 Perimembranous inlet VSD extending to the level of the AV valves (**a**). In this patient, there is overriding of the tricuspid valve annulus over the VSD (**b**). The diastolic frame shows straddling of the tricuspid valve, with partial insertion of the valve apparatus in the left ventricle (**c**)

On the other hand, colour Doppler allows localization of the direction of the jet as a prerequisite of exact quantification of jet velocity by pulsed wave or continuous wave Doppler sonography.

Localization of defects in the membranous, inlet and outlet septum has been already addressed in the preceding paragraph. The parasternal short-axis view, with its different planes from the base of the heart down to the apex, is most important in the detection and description of muscular VSDs. Muscular inlet defects, which are located posterior, can be visualized in a parasternal short axis with a plane through the midportion of the left ventricle (Fig. 3.16, Video 3.23). Muscular inlet defects in this plane are localized at 7–8 o'clock. Another plane for confirmation of posterior defects is the posterior plane of the apical four-chamber view (Fig. 3.16, Video 3.24).

The most favourable plane for visualization of anterior trabecular defects is the parasternal short axis of the midportion of the septum (Fig. 3.17, Videos 3.25 and 3.26) depicting these defects at 2–3 o'clock. Defects in this location can also be visualized from the subcostal window in the subcostal coronal view. Due to their location in the anterior part of the trabecular septum, which approaches the right ventricular outflow tract, visualization of these defects requires a rather anterior orientation of the transducer.

Midventricular defects are easy to visualize. In the midventricular parasternal short-axis view, they appear at 12 o'clock (Video 3.27), and in the apical four-chamber view, they are localized in the midportion of the septum (Fig. 3.18, Videos 3.28 and 3.29). Furthermore they can be detected in the midportion of the ventricular septum in the parasternal long axis (Fig. 3.18, Video 3.30). Apical muscular defects are best visualized in the apical four-chamber view and in parasternal short axis of the apex (Fig. 3.19, Videos 3.31 and 3.32).

Irrespective of the localization of ventricular septal defects, bidirectional shunting is frequently present in the neonatal period due to physiologically elevated pulmonary artery pressure and resistance. Detection of bidirectional shunting by colour Doppler interrogation requires frame-by-frame analysis of a cine loop (Fig. 3.3, Video 3.33). After the first weeks of life, bidirectional shunting usually disappears

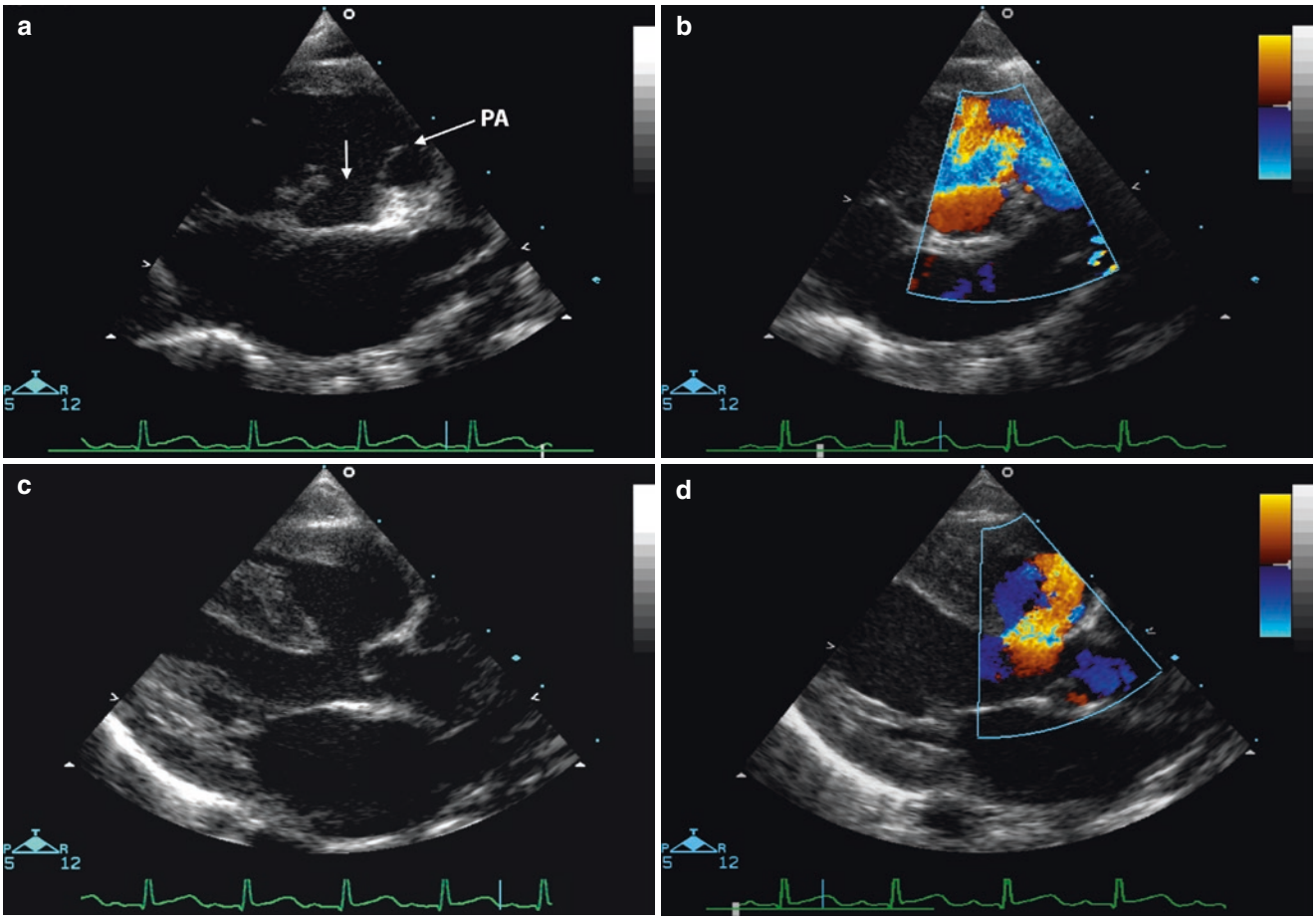

Fig. 3.13 Parasternal short-axis view (**a**) showing a doubly committed VSD (*arrow*), which extends superiorly up to the pulmonary valve (PA). Significant LR-shunting is evident on colour Doppler (**b**). In the parasternal long-axis view, the large defect is located underneath the aortic valve (**c**) with LR-shunting on colour Doppler (**d**)

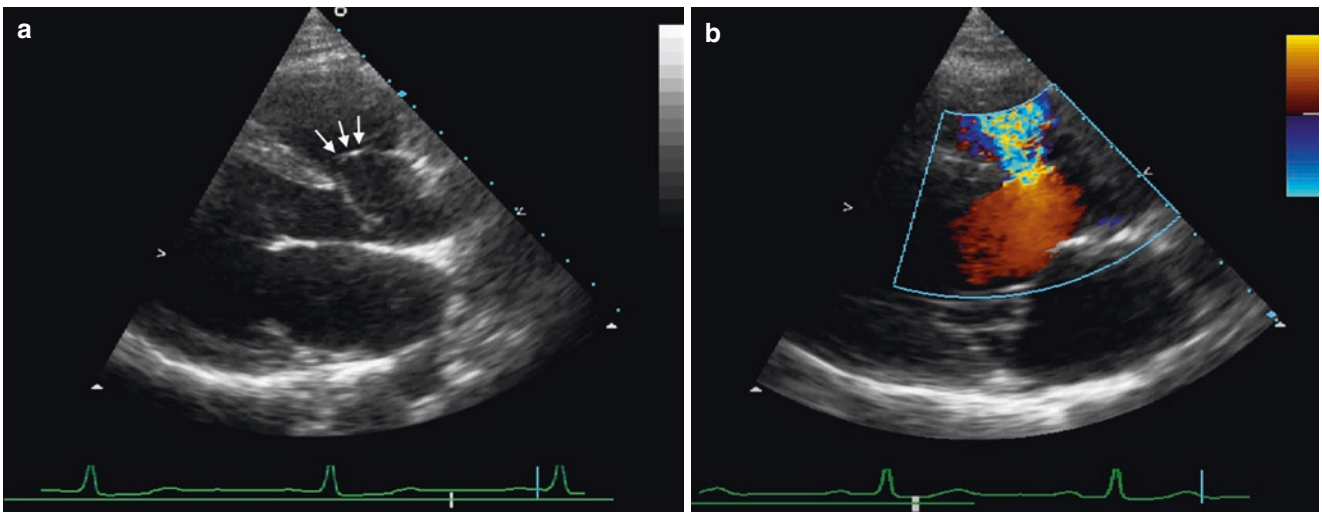

Fig. 3.14 Parasternal long-axis view showing prolapse of the right coronary cusp of the aortic valve (*arrows*) in a patient with a small doubly committed VSD (**a**). Colour Doppler reveals LR-shunting across the defect underneath the aortic valve (**b**)

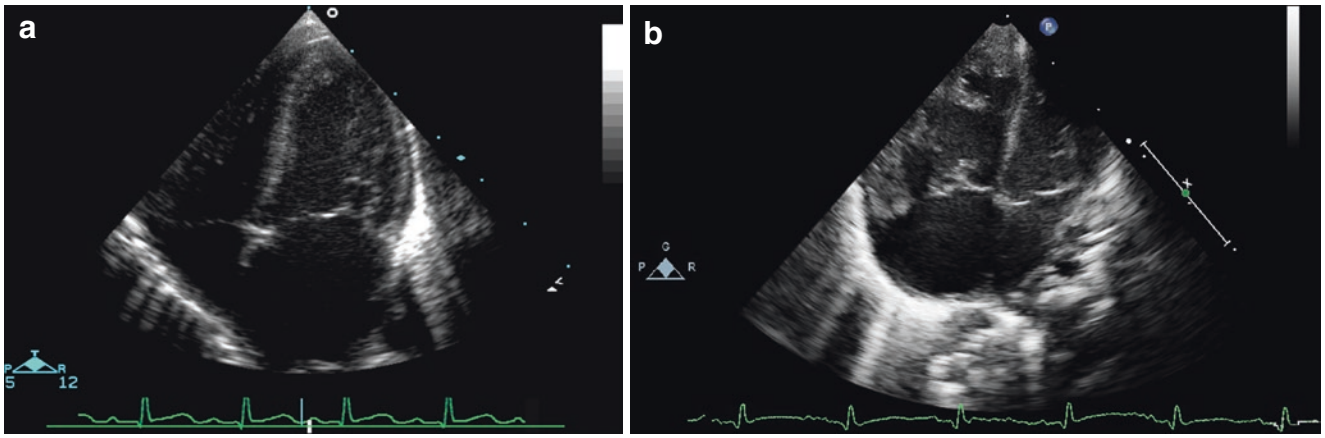

Fig. 3.15 Apical four-chamber view in a patient with large perimembranous VSD and low pulmonary vascular resistance exhibits dilatation of the left atrium and ventricle due to excessive LR-shunting (**a**). In a patient with perimembranous VSD and elevated pulmonary vascular resistance, the right ventricle is hypertrophied and enlarged (**b**)

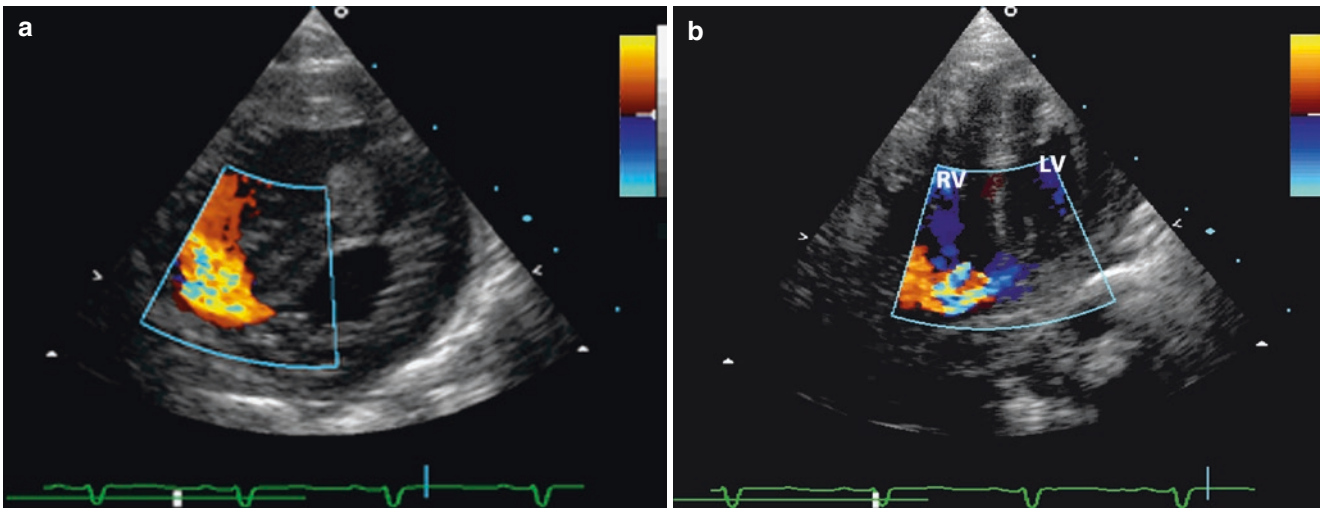

Fig. 3.16 Colour Doppler examination in the parasternal short-axis view showing a muscular inlet VSD (**a**). Visualization of the defect in the four-chamber view requires a posterior orientation of the transducer (**b**). *LV* left ventricle, *RV* right ventricle

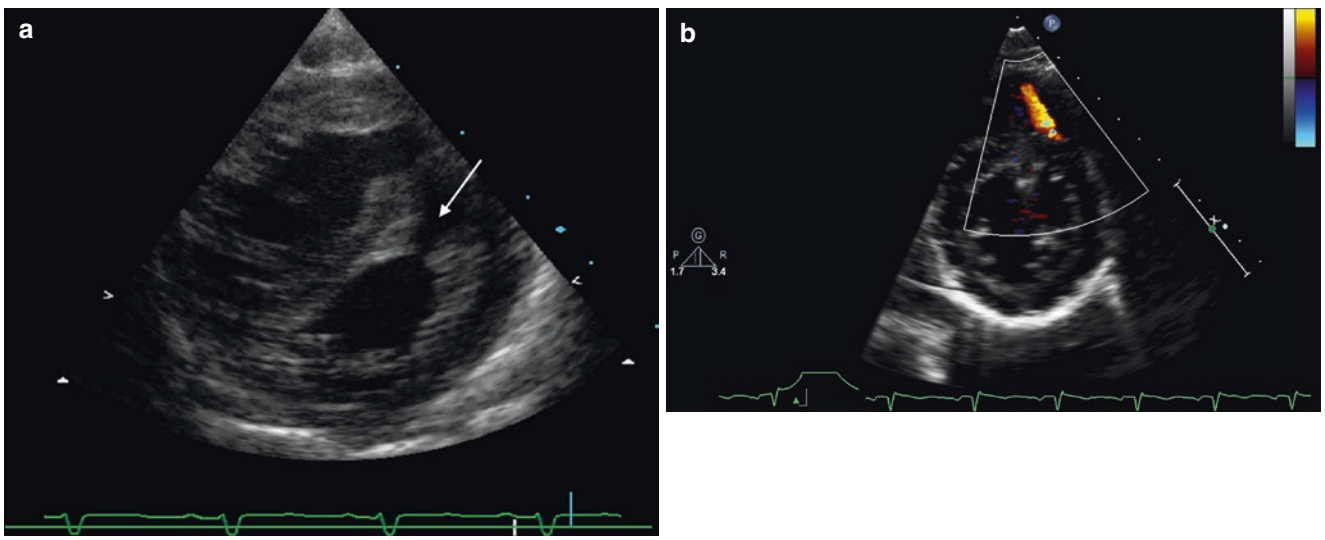

Fig. 3.17 Large anterior muscular VSD (*arrow*) in the parasternal short-axis view (**a**); colour Doppler in the same plane shows LR-shunting in a patient with a small restrictive defect (**b**)

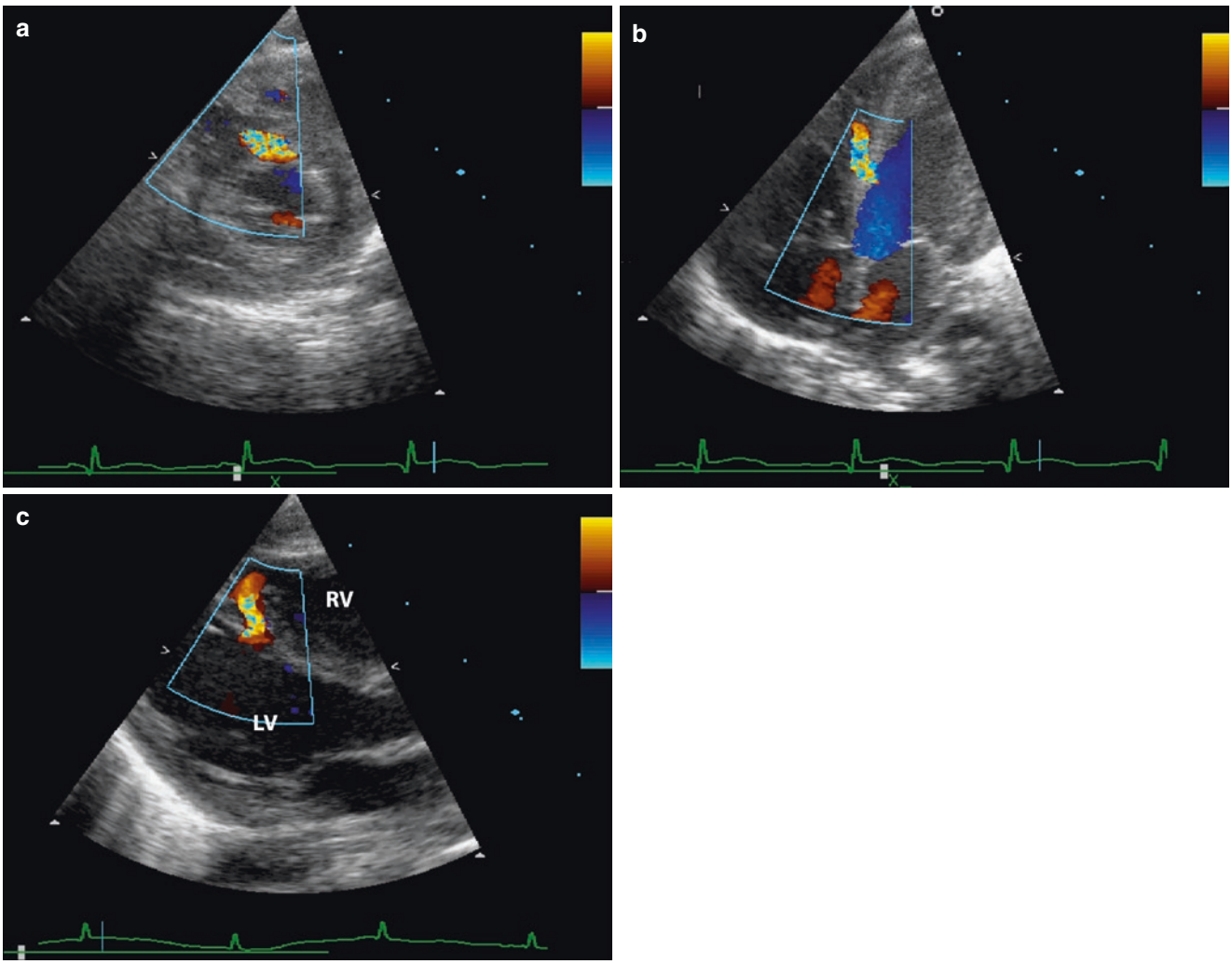

Fig. 3.18 Restrictive midventricular VSD in the parasternal short-axis view (**a**), the apical four-chamber view (**b**) and in the parasternal long-axis view (**c**). *LV* left ventricle, *RV* right ventricle

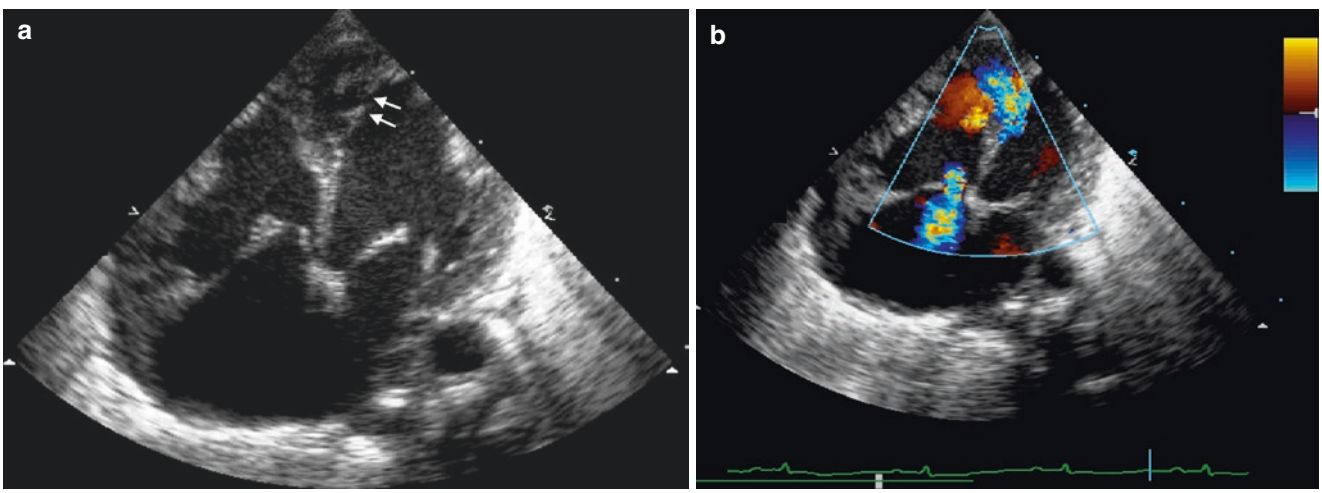

Fig. 3.19 Large apical muscular VSD (*arrows*) in the apical four-chamber view (**a**). Colour Doppler confirms significant shunting across the defects and shows tricuspid regurgitation (**b**)

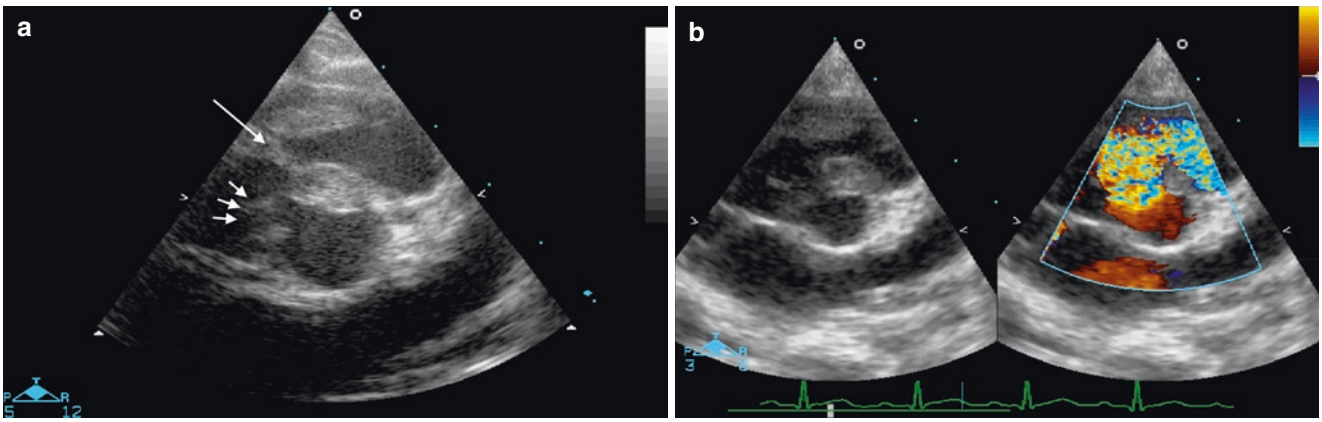

Fig. 3.20 Parasternal short axis of the base of the heart showing a perimembranous VSD (**a**), which is partially occluded by accessory tricuspid valve tissue (*arrows*). In addition there is obstruction of the right ventricular outflow tract by anomalous muscle bundles (*large arrow*). Colour Doppler confirms accelerated flow across the defect and in the outflow tract (**b**)

due to the decline of pulmonary vascular resistance. Beyond the neonatal period, almost all ventricular septal defects present with preferential or exclusive LR-shunting. *Persistence or reappearance of bidirectional shunting is a strong indicator for elevation of pulmonary arterial resistance*.

Depending on their size, VSDs will either be large enough to allow equalization of ventricular pressures or, in the case of smaller defects, have restrictive qualities maintaining a significant pressure gradient between both ventricles. Quantification of these pressure gradients is a domain of pulsed wave and continuous wave Doppler. For confirmation of spontaneous closure, which is frequent especially in small muscular defects (Penny and Vick 2011; Ramaciotti et al. 1995; Roguin et al. 1995), colour Doppler is the method of choice.

Colour Doppler also plays a significant role in the detection of additional cardiovascular malformations that have to be screened systematically in the long-term follow-up of patients with small perimembranous VSDs that do not require surgical closure for haemodynamic reasons. *These problems that may develop in the course of time are aortic regurgitation, double-chambered right ventricle due to anomalous muscle bundles and subaortic stenosis* (Penny and Vick 2011).

- Since perimembranous VSDs are in close proximity to the aortic valve, the jet of the VSD may compromise the valve resulting in prolapse of the right or noncoronary cusp with consecutive aortic regurgitation (Tweddell et al. 2006). The detection of aortic valve regurgitation should prompt surgical closure of the defect to avoid progressive damage of the valve (Saleeb et al. 2007; Tweddell et al. 2006). This applies also for small defects, which would not require surgical closure for haemodynamic reasons. Aortic valve prolapse is even more frequent in patients with subarterial, doubly committed VSDs (Craig et al. 1986; Momma et al. 1984; Schmidt et al. 1988). These defects however are rare in Europe among the Caucasian population (Fig. 3.14). *To detect early signs of aortic valve prolapse and aortic regurgitation, the aortic valve should be screened carefully in the parasternal long and short axis views in all patients with perimembranous or subarterial VSDs*.
- Subvalvular right ventricular outflow tract obstruction due to anomalous muscle bundles may develop and cause progressive subpulmonary stenosis (see Chap. 7). Since these muscle bundles result in the division of the right ventricle into a proximal high-pressure and a distal low-pressure compartment, this anomaly has been termed "double-chambered right ventricle" (Galal et al. 2000; Vogel et al. 1988; Restivo et al. 1984). Turbulence and acceleration of blood flow can be detected by CDE in the parasternal short-axis and in the subcostal views of the RVOT (Fig. 3.20).
- Obstruction of the left ventricular outflow tract may develop due to development of a progressive fibromuscular shelf underneath the aortic valve. Although the exact nature of the development of this stenosis is not understood yet, abnormal haemodynamics and turbulence in the outflow tract seem to play a significant role (Vogel et al. 1988; Baumstark et al. 1978). CDE in the parasternal long-axis and in the apical five-chamber view demonstrates turbulence and acceleration of blood flow in the subaortic region. Careful examination of the subaortic region by 2DE confirms the presence of a subaortic membrane (see Chap. 19).

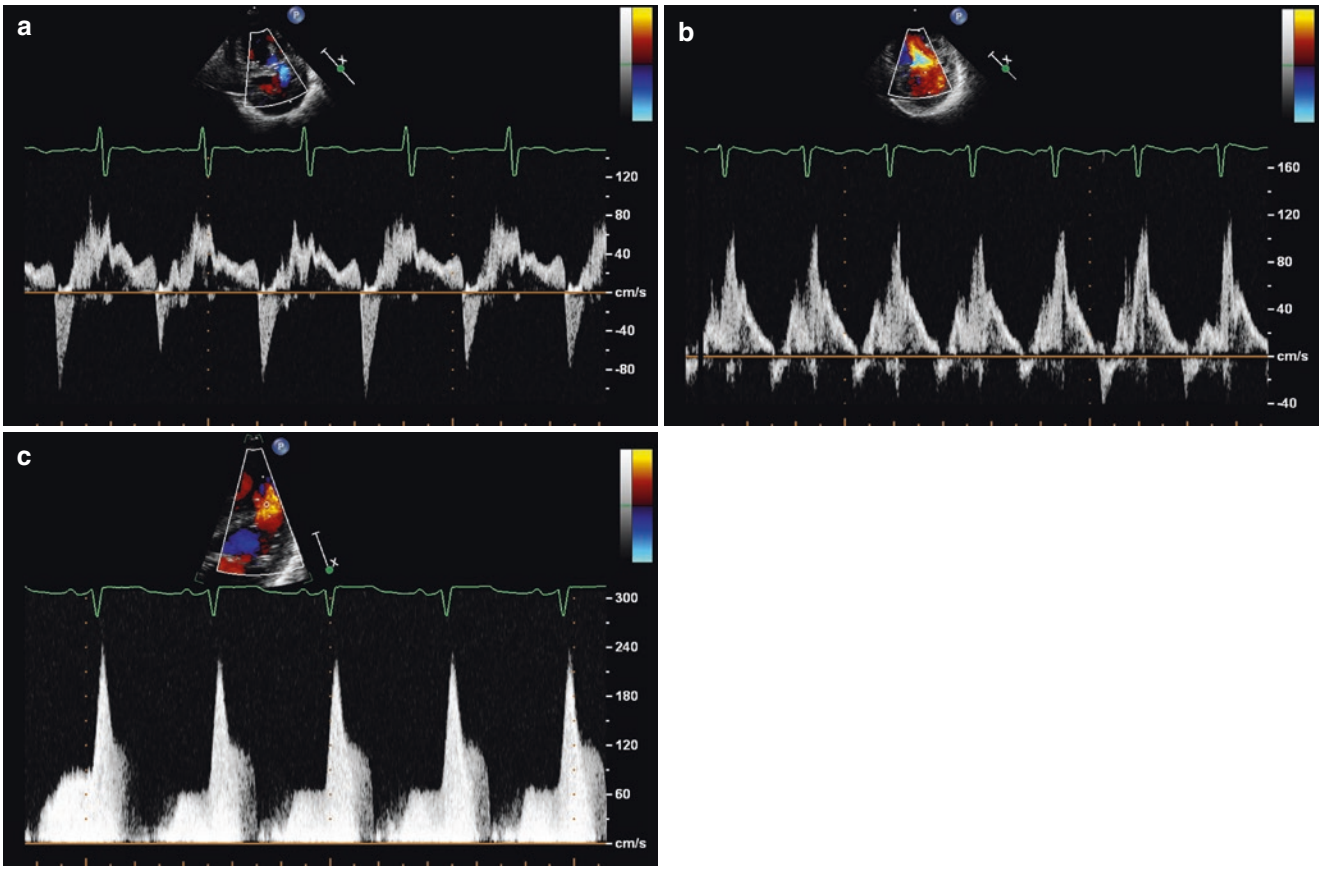

Fig. 3.21 Pulsed wave Doppler of a large muscular VSD (parasternal short axis) in a neonate shows bidirectional shunting at low flow velocities (**a**); with decreasing pulmonary vascular resistance, shunting pattern changes into predominant (**b**) and later into exclusive LR-shunting (**c**)

3.4 Pulsed Wave and Continuous Wave Doppler Sonography

Pulsed wave and continuous Doppler are essential tools in the noninvasive haemodynamic assessment of ventricular septal defects, since they allow quantification of the direction, velocity and duration of shunting across the defect. VSD represents a communication between two fluid-filled systems. Shunting between these spaces will be related on one hand to the pressure difference between both compartments. In the presence of equal pressures in both ventricles, there will be shunting at low flow velocities across the defect which can be well displayed by pulsed wave Doppler. This is the case in patients with large VSDs, approximating the diameter of the aortic valve. In the neonatal period, when pulmonary vascular resistance is still elevated physiologically, patients with large defects frequently present a bidirectional pattern of shunting (Fig. 3.21). With decreasing pulmonary vascular resistance after the first weeks of life, the shunting pattern changes to an exclusive LR-shunting. If the VSD remains large and continues to allow equalization of pressures in both ventricles, flow velocities across the defect will remain below 3 m/s (Fig. 3.21).

Medium-size and small VSDs do not allow transmission of the systemic left ventricular pressure to the right ventricle resulting in a pressure difference between both ventricles. According to this pressure gradient, blood flow passing the VSD will do this with significantly accelerated flow velocities. The measurement of these velocities exceeding 3 m/s requires the application of CW Doppler (Fig. 3.22). The pressure difference between both ventricles can be calculated based on the maximal flow velocity across the VSD with the simplified Bernoulli equation (Marx et al. 1985; Murphy et al. 1986).

$$\text{Gradient across VSD} = 4v^2$$

In addition this equation allows noninvasive estimation of systolic RV pressure: in the absence of obstruction of the left ventricular outflow tract, the systolic blood pressure (which can be measured noninvasively) equals the systolic pressure in the left ventricle. The systolic right ventricular pressure can be obtained by subtraction of the gradient across the VSD from the systolic left ventricular pressure.

$$\text{Systolic pressure RV} = \text{Systolic blood pressure} - \text{gradient across VSD}$$

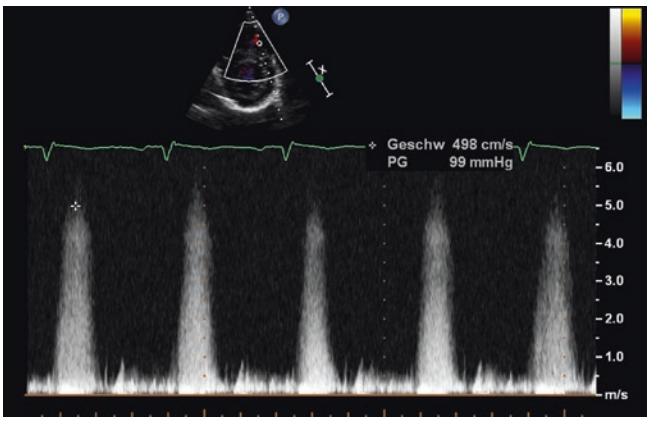

Fig. 3.22 Continuous wave Doppler in a patient with restrictive muscular VSD measures a maximal flow velocity of 4.98 m/s. According to the simplified Bernoulli equation, this represents a systolic pressure gradient of 99 mmHg between the left and right ventricle

In the absence of a gradient between the right ventricle and the pulmonary arteries, the systolic RV pressure will be identical to the systolic pulmonary artery pressure. Precondition of these calculations is a reliable quantification of the maximal flow velocity across the defect. It can be measured only if there is optimal alignment of Doppler beam with the bloodstream crossing the defect. Since this blood flow may be eccentric, the exact measurement requires knowledge of the blood flow direction. Doppler interrogation of the defect should be performed always in conjunction with CDE, which allows selection of the optimal plane to enable good alignment of the Doppler beam with the jet across the VSD.

Ventricular septal defects may undergo spontaneous decrease in size or even spontaneous closure. This applies specifically for muscular or perimembranous defects. In the latter defects, it is frequently accessory tricuspid valve tissue that results in progressive restriction of the defect. This is reflected by increasing flow velocities and increasing gradients between both ventricles. As a rule of thumb, it can be assumed that a significant pressure drop between both ventricles, making pulmonary hypertension unlikely, is present if the flow velocity across the defect exceeds 4 m/s (Fig. 3.22).

Noninvasive calculation of the ratio of pulmonary to systemic flow is theoretically possible (Kurokawa et al. 1988; Sanders et al. 1983; Vargas Barron et al. 1984). It requires quantification of flow both in the pulmonary artery and in the aorta by pulsed wave Doppler sonography as well as measurement of the area of the respective vessels. However this calculation does not play a significant role in the clinical assessment of children with VSD due its inaccuracy, which can be attributed to a large extent to the difficulty of exact quantification of the area of aorta and pulmonary artery (Snider et al. 1997).

References

Baker EJ, Leung MP et al (1988) The cross sectional anatomy of ventricular septal defects: a reappraisal. Br Heart J 59(3):339–351

Baumstark A, Fellows KE et al (1978) Combined double chambered right ventricle and discrete subaortic stenosis. Circulation 57(2):299–303

Butter A, Duncan W et al (1998) Aortic cusp prolapse in ventricular septal defect and its association with aortic regurgitation – appropriate timing of surgical repair and outcomes. Can J Cardiol 14(6):833–840

Capelli H, Andrade JL et al (1983) Classification of the site of ventricular septal defect by 2-dimensional echocardiography. Am J Cardiol 51(9):1474–1480

Craig BG, Smallhorn JF et al (1986) Cross-sectional echocardiography in the evaluation of aortic valve prolapse associated with ventricular septal defect. Am Heart J 112(4):800–807

Galal O, Al-Halees Z et al (2000) Double-chambered right ventricle in 73 patients: spectrum of the disease and surgical results of transatrial repair. Can J Cardiol 16(2):167–174

Jacobs JP, Burke RP et al (2000) Congenital Heart Surgery Nomenclature and Database Project: ventricular septal defect. Ann Thorac Surg 69(4 Suppl):S25–S35

Kaulitz R, Jonas RA et al (1999) Echocardiographic assessment of interrupted aortic arch. Cardiol Young 9(6):562–571

Kelle AM, Young L et al (2009) The Gerbode defect: the significance of a left ventricular to right atrial shunt. Cardiol Young 19(Suppl 2):96–99

Kurokawa S, Takahashi M et al (1988) Noninvasive evaluation of the ratio of pulmonary to systemic flow in ventricular septal defect by means of Doppler two-dimensional echocardiography. Am Heart J 116(4):1033–1044

Leung MP, Mok CK et al (1986) An echocardiographic study of perimembranous ventricular septal defect with left ventricular to right atrial shunting. Br Heart J 55(1):45–52

Lindinger A, Schwedler G et al (2010) Prevalence of congenital heart defects in newborns in Germany: results of the first registration year of the PAN Study (July 2006 to June 2007). Klin Padiatr 222(5): 321–326

Ludomirsky A, Huhta JC et al (1986) Color Doppler detection of multiple ventricular septal defects. Circulation 74(6):1317–1322

Marx GR, Allen HD et al (1985) Doppler echocardiographic estimation of systolic pulmonary artery pressure in pediatric patients with interventricular communications. J Am Coll Cardiol 6(5): 1132–1137

Momma K, Toyama K et al (1984) Natural history of subarterial infundibular ventricular septal defect. Am Heart J 108(5):1312–1317

Murphy DJ Jr, Ludomirsky A et al (1986) Continuous-wave Doppler in children with ventricular septal defect: noninvasive estimation of interventricular pressure gradient. Am J Cardiol 57(6):428–432

Nygren A, Sunnegardh J et al (2000) Preoperative evaluation and surgery in isolated ventricular septal defects: a 21 year perspective. Heart 83(2):198–204

Penny DJ, Vick GW 3rd (2011) Ventricular septal defect. Lancet 377(9771):1103–1112

Ramaciotti C, Vetter JM et al (1995) Prevalence, relation to spontaneous closure, and association of muscular ventricular septal defects with other cardiac defects. Am J Cardiol 75(1):61–65

Restivo A, Cameron AH et al (1984) Divided right ventricle: a review of its anatomical varieties. Pediatr Cardiol 5(3):197–204

Rhodes LA, Keane JF et al (1990) Long follow-up (to 43 years) of ventricular septal defect with audible aortic regurgitation. Am J Cardiol 66(3):340–345

Roguin N, Du ZD et al (1995) High prevalence of muscular ventricular septal defect in neonates. J Am Coll Cardiol 26(6):1545–1548

Saleeb SF, Solowiejczyk DE et al (2007) Frequency of development of aortic cuspal prolapse and aortic regurgitation in patients with subaortic ventricular septal defect diagnosed at <1 year of age. Am J Cardiol 99(11):1588–1592

Sanders SP, Yeager S et al (1983) Measurement of systemic and pulmonary blood flow and QP/QS ratio using Doppler and two-dimensional echocardiography. Am J Cardiol 51(6):952–956

Schmidt KG, Cassidy SC et al (1988) Doubly committed subarterial ventricular septal defects: echocardiographic features and surgical implications. J Am Coll Cardiol 12(6):1538–1546

Schwedler G, Lindinger A et al (2011) Frequency and spectrum of congenital heart defects among live births in Germany: a study of the Competence Network for Congenital Heart Defects. Clin Res Cardiol 100(12):1111–1117

Smallhorn JF, Anderson RH et al (1982) Cross-sectional echocardiographic recognition of interruption of aortic arch between left carotid and subclavian arteries. Br Heart J 48(3):229–235

Snider RA, Serwer GA et al (1997) Echocardiography in pediatric heart disease. Mosby, St. Louis

Sutherland GR, Godman MJ et al (1982) Ventricular septal defects. Two dimensional echocardiographic and morphological correlations. Br Heart J 47(4):316–328

Tweddell JS, Pelech AN et al. (2006). Ventricular septal defect and aortic valve regurgitation: pathophysiology and indications for surgery. Semin Thorac Cardiovasc Surg Pediatr Card Surg Annu 9(1):147–152

Vargas Barron J, Sahn DJ et al (1984) Clinical utility of two-dimensional doppler echocardiographic techniques for estimating pulmonary to systemic blood flow ratios in children with left to right shunting atrial septal defect, ventricular septal defect or patent ductus arteriosus. J Am Coll Cardiol 3(1):169–178

Vogel M, Smallhorn JF et al (1988) An echocardiographic study of the association of ventricular septal defect and right ventricular muscle bundles with a fixed subaortic abnormality. Am J Cardiol 61(10): 857–860

Yoshimura N, Hori Y et al (2010) Comparison of magnetic resonance imaging with transthoracic echocardiography in the diagnosis of ventricular septal defect-associated coronary cusp prolapse. J Magn Reson Imaging 32(5):1099–1103